Title

Antitumor activity of a lectibody targeting cancer-associated high-mannose glycans

Journal

Molecular Therapy, 30(4)

ISSN

1525-0016

Authors

Oh, Young Jun
Dent, Matthew W
Freels, Angela R
et al.

Publication Date

2022-04-01

DOI

10.1016/j.ymthe.2022.01.030

Peer reviewed

Molecular Therapy
Original Article

Antitumor activity of a lectibody targeting cancer-associated high-mannose glycans

Young Jun Oh,[1] Matthew W. Dent,[1,2] Angela R. Freels,[1] Qingwen Zhou,[3] Carlito B. Lebrilla,[3] Michael L. Merchant,[4] and Nobuyuki Matoba[1,2,5]

[1]UofL Health - Brown Cancer Center, University of Louisville School of Medicine, 505 S. Hancock Street, Louisville, KY 40202, USA; [2]Department of Pharmacology and Toxicology, University of Louisville School of Medicine, Louisville, KY, USA; [3]Department of Chemistry, University of California Davis, Davis, CA 95616, USA; [4]Division of Nephrology and Hypertension, Department of Medicine, University of Louisville School of Medicine, KY, USA; [5]Center for Predictive Medicine, University of Louisville School of Medicine, Louisville, KY, USA

Aberrant protein glycosylation is a hallmark of cancer, but few drugs targeting cancer glycobiomarkers are currently available. Here, we showed that a lectibody consisting of the high-mannose glycan-binding lectin Avaren and human immunoglobulin G1 (IgG1) Fc (AvFc) selectively recognizes a range of cell lines derived from lung, breast, colon, and blood cancers at nanomolar concentrations. Binding of AvFc to the non-small cell lung cancer (NSCLC) cell lines A549 and H460 was characterized in detail. Co-immunoprecipitation proteomics analysis revealed that epidermal growth factor receptor (EGFR) and insulin-like growth factor 1 receptor (IGF1R) are among the lectibody's common targets in these cells. AvFc blocked the activation of EGFR and IGF1R by their respective ligands in A549 cells and inhibited the migration of A549 and H460 cells upon stimulation with EGF and IGF1. Furthermore, AvFc induced potent Fc-mediated cytotoxic effects and significantly restricted A549 and H460 tumor growth in severe combined immunodeficiency (SCID) mice. Immunohistochemistry analysis of primary lung tissues from NSCLC patients demonstrated that AvFc preferentially binds to tumors over adjacent non-tumor tissues. Our findings provide evidence that increased abundance of high-mannose glycans in the glycocalyx of cancer cells can be a druggable target, and AvFc may provide a new tool to probe and target this tumor-associated glycobiomarker.

INTRODUCTION

It has become evident that changes in protein glycosylation patterns are associated with various disease conditions, including viral infections and cancer.[1,2] One such change observed in several cancer types is a significant increase in the proportion of high-mannose-type glycans, which constitute a type of asparagine-linked glycan (*N*-glycan) containing 5–9 terminal mannose residues.[2,3] In normal cells, these glycoforms appear in the endoplasmic reticulum (ER) but are subsequently processed into complex-type glycans by a series of mannosidases and glycosyltransferases in the Golgi apparatus as nascent glycoproteins passage through the secretory pathway. Thus, high-mannose glycans are considered to be "immature" *N*-glycans that are generally confined in the ER under normal conditions.[1] However, recent studies based on quantitative mass spectrometry analyses of cancer tissue have demonstrated that this may not always be the case. For example, high-mannose glycans were elevated in serum samples from breast cancer patients, which correlated with cancer progression.[4] Analysis of large cohorts of paired breast cancerous and adjacent non-tumor tissues found a high-mannose glycan (Man8) along with a triantennary glycan to be dramatically increased in the membrane fraction of tumors.[5] Increased abundance of high-mannose glycans has also been observed in colorectal tumor tissues,[6–8] hepatocellular carcinoma,[9,10] metastatic cholangiocarcinoma,[11] lung adenocarcinoma,[12] pancreatic cancer,[13] ovarian cancer,[14,15] prostate cancer,[16] and skin basal cell carcinoma and squamous cell carcinoma.[17] Collectively, the aberrant increase of high-mannose glycans on malignant cells may provide a unique biomarker for drug development. Nevertheless, there are few agents that can distinguish tumor-associated high-mannose glycans from other glycoforms present on the surface of a normal cell, and thus their druggability remains unclear.

Previously, we reported the creation of an antibody-like lectibody molecule comprised of the oligomannose-specific Avaren lectin and the Fc region of human immunoglobulin G1 (IgG1), called Avaren-Fc (AvFc).[18] Avaren is an engineered variant of the actinomycete-derived antiviral lectin actinohivin,[19,20] with amino acid substitutions to improve solubility and producibility. AvFc neutralized the infectivity of multiple HIV strains and hepatitis C viruses (HCVs) at nanomolar concentrations through high-affinity binding to high-mannose glycans clustered on their envelope glycoproteins.[18,21] Additionally, the lectibody exhibited antibody-dependent cell-mediated virus inhibition against HIV-infected peripheral blood mononuclear cells (PBMCs) via its capacity to interact with activating Fcγ receptors such as FcγRI and FcγRIIIa. Preliminary safety studies in mice and rhesus macaques showed that systemic administration of AvFc did

Received 5 May 2021; accepted 20 January 2022; Published: April 06, 2022.
https://doi.org/10.1016/j.ymthe.2022.01.030.

Correspondence: Nobuyuki Matoba, James Graham Brown Cancer Center, University of Louisville School of Medicine, 505 S. Hancock Street, Room 615, Louisville, KY 40202, USA.
E-mail: n.matoba@louisville.edu

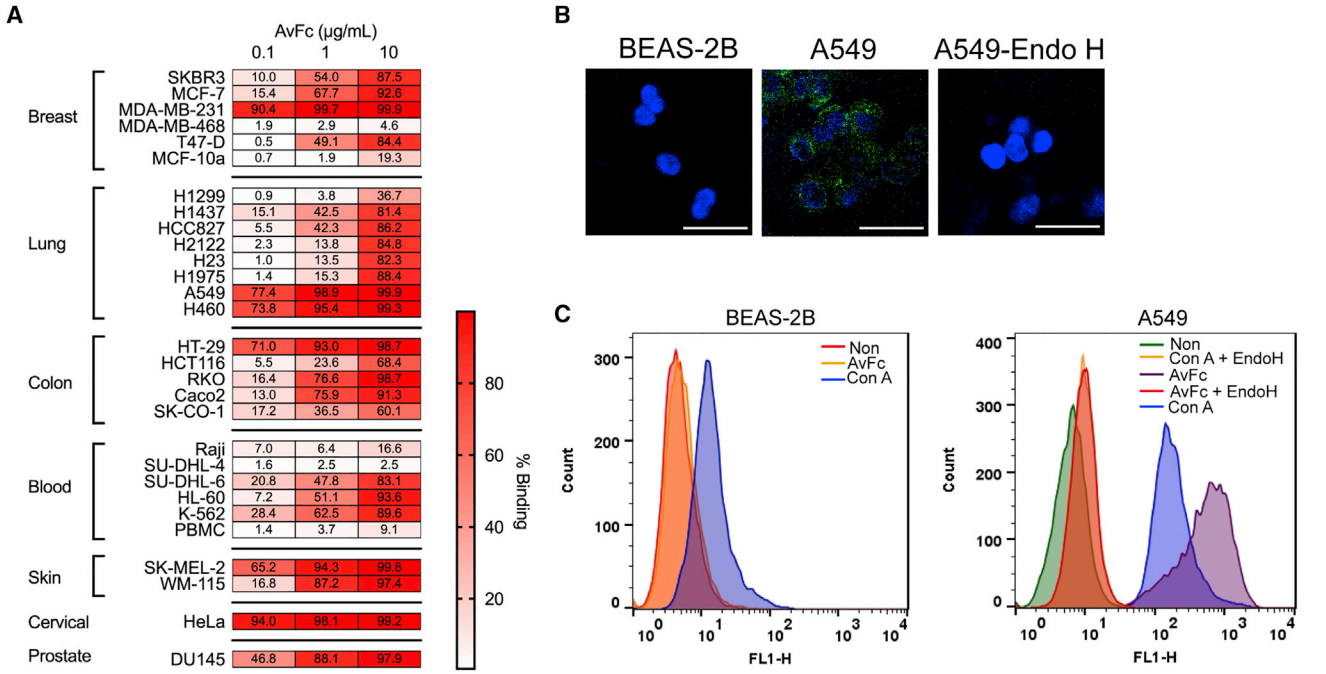

Figure 1. AvFc recognizes high-mannose glycans on cancer cell lines

(A) Binding of AvFc to various cancer cell lines, normal human peripheral blood mononuclear cells (PBMCs), and non-tumorigenic cell lines was evaluated by flow cytometry with 0.1 μg/mL, 1 μg/mL, or 10 μg/mL of drug. The percentages of $FITC^+$ cells are shown as a heatmap, with most cell lines becoming saturated at 10 μg/mL. (B) Immunofluorescence was used to visualize the binding of 1 μg/mL of AvFc to the non-tumorigenic lung epithelial cell line BEAS-2B and to A549 cells with or without endoglycosidase H (Endo H) treatments. AvFc does not show any binding to BEAS-2B or to endo H-treated A549 cells. Scale bar, 20 μm. (C) Flow cytometry of BEAS-2B and A549 after staining with either AvFc or Con A shows that Con A can weakly bind to both BEAS-2B and A549 cells and that endo H digestion of cells abrogates binding by both lectins.

not induce any discernible toxicity.[18] Furthermore, systemic administration of 25 mg/kg of AvFc every other day (Q2D) for 14 or 20 days (8 or 11 doses total, respectively) completely protected against HCV challenge without causing hepatotoxicity or any other significant adverse effects in a chimeric human liver mouse model.[21] These results lend support for the use of AvFc in novel therapeutic strategies targeting high-mannose glycans that may loom on the cell surface in high densities under pathological conditions.

In light of growing evidence for the aberrant overexpression of high-mannose glycans in neoplastic cells, we hypothesized that AvFc could efficiently recognize these mannose-rich glycans on the surface of cancer cells and thereby exhibit antitumor activity. To address this hypothesis, the present study investigated the capacity of the lectibody to target cancer using human non-small cell lung cancer (NSCLC) cell lines, murine xenograft models of human NSCLC, and primary human NSCLC tissue sections. Our results provide implications for a novel anticancer strategy targeting tumor-associated high-mannose glycans.

RESULTS

AvFc selectively recognizes various cancer cell lines

Given that high-mannose glycans are elevated in various neoplastic cells and tissues,[4–7,9,12–16] we first tested whether AvFc can effectively recognize cancer cells. Flow cytometry analysis showed that the lectibody bound to a range of human cancer cell lines derived from breast, lung, colon, blood, cervical, and prostate tumors at nanomolar concentrations. Nanomolar concentrations (0.1–10 μg/mL) of AvFc exhibited distinct binding to most of the 27 cancer cell lines tested, albeit with varying degrees of efficiency. MDA-MB-231 breast carcinoma, A549 lung adenocarcinoma, H460 large-cell lung carcinoma, HT-29 colon adenocarcinoma, SK-MEL-2 melanoma, and HeLa cervical carcinoma cell lines are among those most prominently recognized by the lectibody even at the lowest concentration (i.e., 0.1 μg/mL or 1.3 nM) analyzed (Figure 1A). By contrast, AvFc poorly recognized normal human PBMCs and non-tumorigenic cell lines, including MCF10 mammary gland epithelial and BEAS-2B lung epithelial cells. Marginal binding was also noted for relatively few cancer cell lines, including MDA-MB-468 breast carcinoma, Raji Burkitt lymphoma, and SU-DHL-4 B cell lymphoma cells (Figures 1A–1C).

When A549 cells were treated with endoglycosidase H (Endo H), which specifically cleaves high-mannose glycans,[22] the binding of AvFc to the cell line was almost completely abolished (Figures 1B and 1C). Additionally, binding of the lectibody to A549 cells was inhibited in a dose-dependent manner by yeast mannan and the HIV-1 envelope glycoprotein gp120 (Figure S1). These results demonstrate that interaction of AvFc with cancer cells is mediated via the

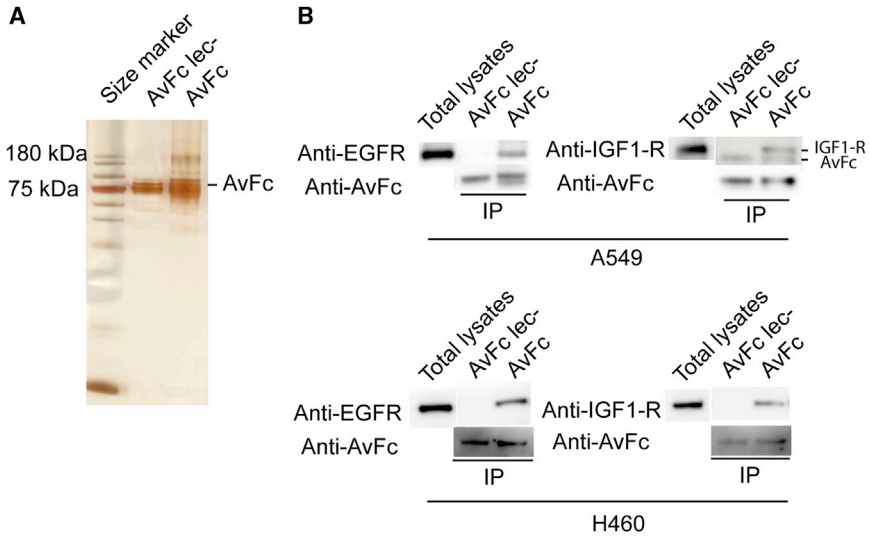

Figure 2. Identification of cancer cell surface binding partners of AvFc

Potential binding partners were isolated using co-immunoprecipitation and identified using mass spectrometry. (A) Silver staining of AvFc and AvFc^{lec-} fractions obtained after co-immunoprecipitation. In addition to the band corresponding to AvFc itself (≈77 kDa), other species at higher and lower molecular weights are present suggesting that AvFc successfully pulled down potential binding partners. (B) Co-immunoprecipitation was used to confirm the interaction between AvFc and EGFR/IGF1R isolated from A549 and H460 cells. Pulldown with AvFc and then blotting with anti-EGFR or anti-IGFR antibodies revealed that AvFc, but not AvFc^{lec-}, interacts with EGFR and IGF1R derived from both cell lines. Note that a longer exposure time for IGF1R in A549, which was necessary due to low expression of the receptor, resulted in the detection of AvFc and AvFc^{lec-} in the blot owing to cross-reactivity of the detection antibody.

high-mannose-binding activity of the lectibody's lectin domain. The mannose-binding lectin concanavalin A (Con A) also strongly recognized A549 cells, and similar to AvFc, this interaction was disrupted by Endo H digestion of cell-surface glycans. In contrast to AvFc, however, Con A exhibited a relatively weak yet appreciable degree of interaction with the non-tumorigenic BEAS-2B cells (Figure 1C), highlighting distinct glycan recognition mechanisms between the lectibody and the canonical legume lectin.

AvFc binds to EGFR and IGF1R and blocks their signaling

We continued our investigation using A549 and H460 cells, two representative NSCLC cell lines that exhibited high AvFc binding in flow cytometry analysis (Figure 1A), with a half-maximal effective concentration of approximately 42 ng/mL for A549 and 30 ng/mL for H460. To identify the molecular targets of AvFc in these cells, we employed a pull-down assay using protein A beads conjugated with AvFc or AvFc^{lec-}, the latter of which is a variant of the lectibody lacking high mannose-binding activity.[21] Binding partners were isolated from A549 and H460 cell lysates and identified using mass spectrometry. Silver staining revealed unique proteins in the AvFc-bound fraction that were not isolated by the negative control, AvFc^{lec-} (Figure 2A). Proteomics analyses of these fractions showed that AvFc recognized a large number of molecules that are found on the cell surface and in the extracellular matrix (Table S1), with many of these being common between the two NSCLC cell lines. These included laminins, integrins, transporters, and growth factor receptors (Table 1). We focused on two major growth factor receptors, epidermal growth factor receptor (EGFR) and insulin-like growth factor 1 receptor (IGF1R), as they are known to play pivotal roles in NSCLC progression.[23–25] To validate the proteomics results, co-immunoprecipitation immunoblot analysis was performed; the results confirmed interaction between AvFc and these receptors in both A549 and H460 cells (Figure 2B). Because EGFR and IGF1R are dimerized upon ligand binding and phosphorylated to trigger pro-survival signaling cascades,[26–29] we investigated whether AvFc can repress the onset of signal transduction by these receptors. After pre-incubation with AvFc, AvFc^{lec-} or the United States Food and Drug Admininstration (FDA)-approved anti-EGFR monoclonal antibody cetuximab (CTX) in serum-free medium, A549 cells were treated with EGF or IGF1, and phosphorylation status of their respective receptors was analyzed by immunoblot (Figures 3A–3D). The results indicated that AvFc, but not AvFc^{lec-}, blocked the activation of both EGFR and IGF1R as evidenced by a decrease in band intensity of the phosphorylated forms of these receptors (pEGFR and pIGF1R). In contrast, while CTX blocked the activation of EGFR as effectively as AvFc, the EGFR-specific monoclonal antibody failed to inhibit the activation of IGF1R. To test whether AvFc can simultaneously block these receptors, we assessed the inhibition of major downstream signaling pathways shared between EGFR and IGF1R after treating A549 cells with a mixture of EGF and IGF1. Specifically, we evaluated activation of the AKT and mitogen-activated protein kinase (MAPK) pathways that are involved in cell invasion, proliferation, and drug resistance.[30–33] Immunoblot analysis showed that AvFc significantly blunted the phosphorylation of AKT and MAPK1 upon EGF and IGF1 co-treatment, whereas CTX and AvFc^{lec-} failed to show any inhibition (Figures 3E–3G).

AvFc inhibits migration of A549 and H460 cells

The above results indicate that AvFc effectively binds to both EGFR and IGF1R on the cell surface, thereby intercepting their ligands and preventing receptor activation and subsequent AKT and MAPK signaling. Because AKT and MAPK signaling pathways are involved in migration,[34,35] we investigated the effects of AvFc on cell migration using A549 and H460 cells and a transwell culture system, wherein cells were co-incubated with the lectibody and

Table 1. The binding targets of AvFc that are common between A549 and H460 cell lines

UniProt accession	Gene name	Protein name
P00533	EGFR	Epidermal growth factor receptor
Q14517	FAT1	Protocadherin FAT1
P08069	IGF1R	Insulin-like growth factor 1 receptor
P17301	ITGA2	Integrin alpha-2
P18084	ITGB5	Integrin beta-5
P26006	ITGA3	Integrin alpha-3
Q07954	LRP1	Low-density lipoprotein receptor-related protein 1
Q9Y666	SLC12A7	Solute carrier family12 member 7
P56199	ITGA1	Integrin alpha-1
Q9NV96	TMEM30A	Cell-cycle control protein 50A
Q15758	SLC1A5	Neutral amino acid transporter B(0)
Q9UNN8	PROCR	Endothelial protein C receptor
P07942	LAMB1	Laminin subunit beta-1
O15230	LAMA5	Laminin subunit alpha-5
P55268	LAMB2	Laminin subunit beta-2
O00468-3	AGRN	Agrin

subsequently treated with EGF or IGF1 in serum-free medium. These cells were then seeded into transwells, and after 6 h, cells in the bottom chamber were quantified. As shown in Figure 4, AvFc significantly blocked the migration of both cell lines regardless of which growth factor the cells were stimulated with, whereas AvFc^{lec-} failed to show any effect. CTX, on the other hand, effectively inhibited the migration of A549 cells treated with EGF, but not the cells treated with IGF1 (Figure 4A). Additionally, CTX failed to show any effect on the migration of H460 cells, even when the cells were stimulated with EGF (Figure 4B).

AvFc induces ADCC against cancer cells

Next, we investigated the consequences of binding of AvFc to cancer cells from a different angle, asking whether the Fc region of the lectibody can direct antibody-dependent cell-mediated cytotoxicity (ADCC). As ADCC is mediated primarily through natural killer (NK) cells expressing FcγRIIIa, we assessed the Fc-mediated activity of AvFc against A549 and H460 cells using an *in vitro* assay based on FcγRIIIa-activated luciferase expression. As shown in Figure 5A, AvFc activated FcγRIIIa in a dose-dependent manner. AvFc^{lec-}, on the other hand, failed to activate FcγRIIIa at all concentrations tested, demonstrating that the activity is dependent upon AvFc's binding to high-mannose glycans on cancer cells. Of note, AvFc showed significantly higher efficacy against A549 cells than CTX at the top 3 concentrations tested (0.08 μM, 0.40 μM, and 2.00 μM). Moreover, AvFc exhibited remarkable activity (a maximum more than 30-fold above baseline) against H460, while CTX was ineffective for the large cell lung carcinoma cell line (Figure 5A). To confirm the ability of AvFc to induce Fc-mediated cell killing activity, a canonical ADCC assay was performed using human PBMC effector cells and A549 cells as the targets. As shown in Figure 5B, the lectibody showed dose-dependent cell lysis activity against A549 cells; it is of note, however, that the efficacy of the lectibody was nearly twice as high as that of CTX (~80% for AvFc versus ~40% for CTX).

AvFc exhibits antitumor effects in mouse A549 and H460 xenograft models

The antitumor effects of AvFc were evaluated in Prkdc^{scid}/SzJ (severe combined immunodeficiency [SCID]) mice challenged with A549 and H460 xenografts implanted in the hind left flank. Intraperitoneal treatment with 25 mg/kg of AvFc or CTX was initiated day 4 days after tumor challenge and continued every 2 days for a total of 6 doses. AvFc treatment significantly blunted A549 (Figure 6A) and H460 (Figure 6B) tumor growth compared with the vehicle control. On the other hand, CTX showed similar efficacy to AvFc against A549 tumors, but failed to show an effect on the growth of H460 tumors. To further evaluate the antitumor effect of AvFc, mice were intravenously challenged with A549-GFP and subsequently treated with the same dosing regimen as in the flank tumor models. Fluorescence imaging of the lung isolated 18 days after the last dose showed that AvFc significantly inhibited the growth of A549-GFP cells in the lung compared with a vehicle control (Figure 6C). Taken together, these data clearly demonstrated that AvFc has the ability to elicit antitumor activity *in vivo*.

AvFc preferentially binds to human NSCLC tumor tissue

Lastly, we investigated the binding of AvFc to primary tumor and adjacent tissues isolated from human NSCLC patients using immunohistochemistry (IHC). Compared with the adjacent tissue, AvFc binding was more evident in NSCLC tumor (Figure 7A), indicating that the lectibody is capable of distinguishing the differential glycosylation patterns. Among the matched pair tissues from 10 NSCLC patients analyzed, 7 showed significantly higher AvFc binding in tumors than in the adjacent tissue (Figure 7B). Given that EGFR was one of the major molecular targets of AvFc in A549 and H460 (Figure 2), we postulated that tumor selectivity of AvFc found in lung tissues of NSCLC patients may be partly attributed to the receptor. Thus, EGFR was enriched from the tumor and adjacent tissue lysate samples from 5 NSCLC patients (patients 151, 117, 448, 234, 155) using co-immunoprecipitation and then detected with AvFc, CTX, or AvFc^{lec-} by western blot. A representative image of tissue samples from patient 117 is shown in Figure 7C, and relative band intensities between tumor EGFR and the adjacent tissue-derived counterpart are shown in Figure 7D. Although AvFc reacted with both tumor and adjacent tissue EGFRs, it showed a stronger signal with the former (approximately 2-fold on average) (Figure 7D), indicating that the lectibody had higher affinity to tumor-derived EGFR. By contrast, CTX showed bands of similar intensity for tumor and adjacent tissue EGFRs in all 5 tissues tested (Figures 7C and 7D). AvFc^{lec-} failed to probe the receptor from both tumor and adjacent tissues. Taken together, these results indicate that AvFc has preferential binding to NSCLC tumor-derived EGFR over that of the normal lung tissue, while CTX cannot distinguish them.

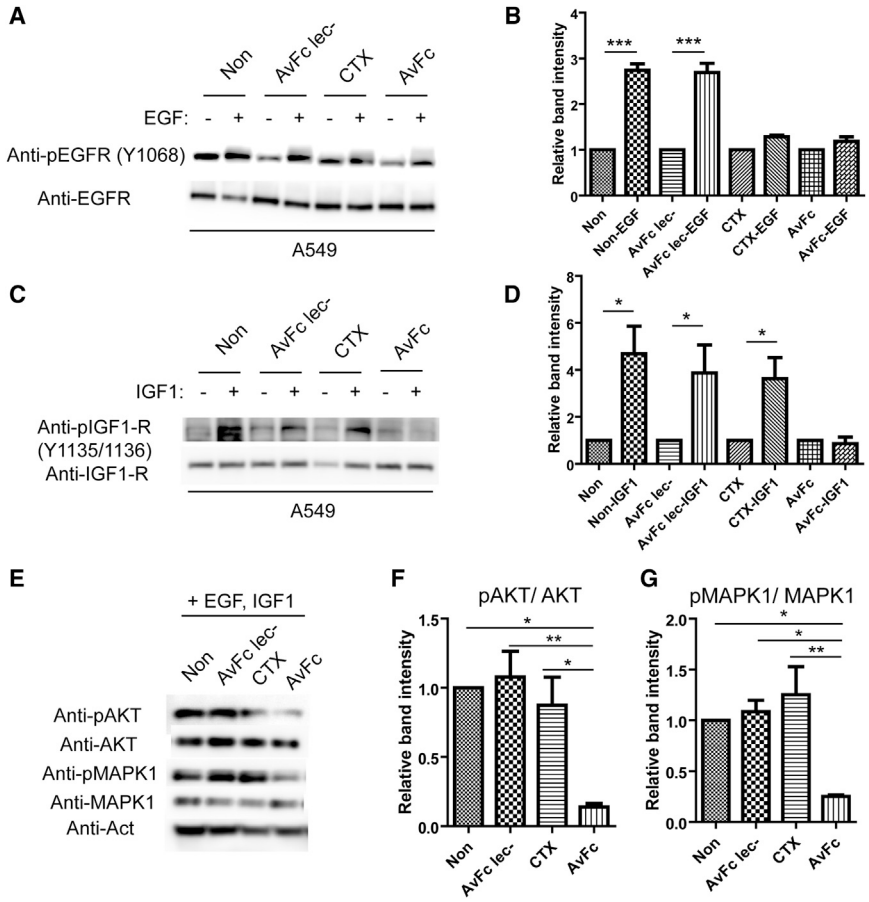

Figure 3. AvFc blocks EGFR and IGF1R signaling

The phosphorylation status of EGFR and IGF1R on A549 cells following treatment with their respective ligands was detected by anti-pEGFR(Y1068) and anti-IGF1R(Y1135/1136) antibodies. (A) Representative immunoblot shows that the treatment of A549 cells with 30 nM of AvFc and CTX, but not AvFc^{lec-}, before the addition of 2 ng/mL of EGF resulted in diminished EGFR activation. (B) Quantification of immunoblot in (A). (C) Representative immunoblot shows that only treatment of A549 cells with 30 nM of AvFc, not CTX or AvFc^{lec-}, before the addition of 2 ng/mL of IGF1 results in decreased activation of IGF1R. (D) Quantification of immunoblot in (C). (E) After incubation of A549 cells with AvFc, CTX or AvFc^{lec-} and subsequent stimulation with a mixture of EGF and IGF1, AKT and MAPK1 phosphorylation was decreased only with AvFc. (F) Quantification of pAKT/AKT in (E). (G) Quantification of pMAPK1/MAPK1 in (E). All relative band intensities were measured by ImageJ. Bars represent mean ± SEM (n = 3). Group means were compared with the two-tailed, unpaired Student t test for (B) and (D) or one-way ANOVA with Bonferroni post-tests for (F and G) (*$p < 0.05$, **$p < 0.01$, ***$p < 0.001$).

DISCUSSION

Aberrant glycosylation has long been recognized as a hallmark of cancer. Nevertheless, development of therapeutics targeting cancer-associated glycans has been slow. In the present study, we showed that AvFc, a lectibody specific to high-mannose glycans,[18] can recognize multiple human cancer cell lines derived from various cancer types. The therapeutic implications of interaction of AvFc with cancer cells were evaluated using two NSCLC cell lines, A549 and H460, demonstrating that the lectibody can block the activation of EGFR and IGF1R and cell migration upon stimulation with their respective ligands, elicit ADCC activity, and significantly delay xenograft tumor growth in SCID mice. Furthermore, IHC analysis showed that AvFc preferentially binds to primary human NSCLC tumors over adjacent non-tumor lung tissues isolated. To our knowledge, this is the first report demonstrating the antitumor effects of an agent targeting cancer-associated high-mannose glycans.

An initial analysis indicated that AvFc has high selectivity to malignant cells over non-cancerous or normal healthy cells, as AvFc did not show any significant binding to non-tumorigenic epithelial cell lines MCF10a and BEAS-2B, human PBMCs (Figures 1A–1C), or primary mesenteric lymph node cells isolated from rhesus macaques.[18] AvFc's specificity to high-mannose glycans has been previously demonstrated by a glycan array analysis using >600 mammalian *N*-glycans,[18] strongly indicating the abnormal accumulation of high-mannose glycans on the surface of cancer cells. Similar results regarding the selectivity for cancer-associated high-mannose glycans were previously reported with TM10, an immunoglobulin M (IgM) monoclonal antibody isolated from mice immunized with FasL-expressing B16F10 mouse melanoma cells.[36] Similar to AvFc, the epitope of TM10 appeared to be clusters of high-mannose glycans, in particular, Man9, and the antibody recognized human melanoma, prostate, ovarian, and breast cancer cells with no apparent surface binding to untransformed cells. However, in contrast to AvFc, TM10 showed little *in vivo* or *in vitro* anticancer activity. The authors attributed the lack of therapeutic effects to the specific isotype of TM10 antibody given that antibodies of IgM isotype typically have poor tissue penetration, have short biological half-lives, and lack Fc-mediated effector functions.[36] Thus, while it appears that selectivity for cancer cells is similar between AvFc and TM10, the presence of the Fc region from IgG1 is the major differentiating factor of AvFc, a molecular design that offers significant advantages as a potential anticancer agent.

Our findings in the present study add to growing evidence indicating that a high proportion of high-mannose glycans represents a unique characteristic of the cancer cell glycocalyx. In contrast to other conventional mannose-binding lectins such as Con A, AvFc preferentially recognizes clusters or groupings of high-mannose glycans containing terminal α1,2-linked mannose residues.[18,21] Such a high density of high-mannose structures is rare in the glycocalyx of

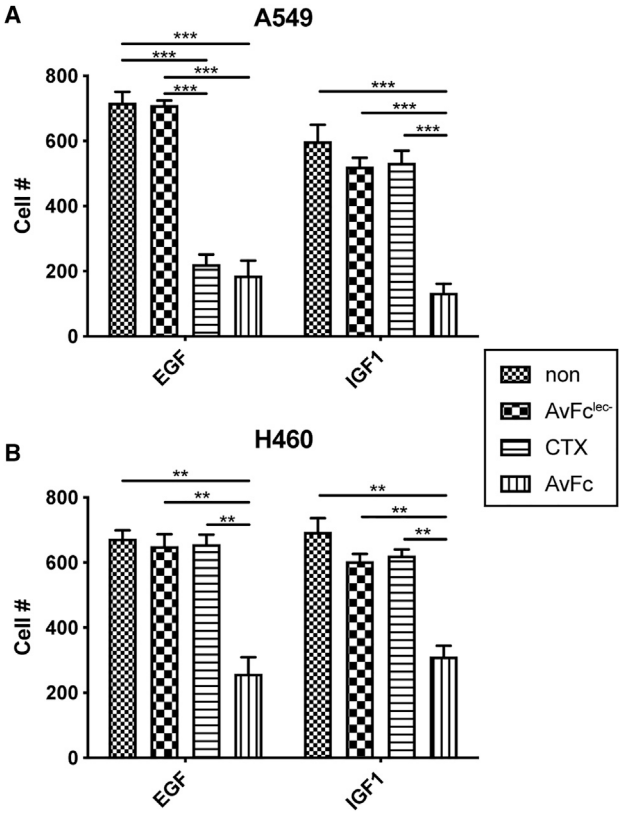

Figure 4. AvFc inhibits A549 and H460 cell migration

(A and B) Migration of A549 cells (A) and H460 cells (B) was measured in transwells with 8 μm pores after treatment of cells with 30 nM of AvFc, CTX, or AvFc^{lec-} and stimulation with EGF or IGF1.

Error bars represent mean ± SEM from 3 replicates. Groups were analyzed by two-way ANOVA followed by Bonferroni multiple comparison test (**$p < 0.01$, ***$p < 0.001$).

normal cells, as illustrated by our data showing the inability of AvFc to recognize the non-tumorigenic BEAS-2B bronchial epithelial cell line, while Con A showed noticeable binding (Figure 1C). Con A interacts with both internal and external α-D-mannosyl and α-D-glucosyl residues and has 4 sugar-binding sites.[37] As such, it is more "promiscuous" than AvFc and capable of recognizing a broader spectrum of glycoforms. Furthermore, preliminary data suggest that AvFc has low affinity to individual glycans and glycoproteins with small numbers of glycans but high affinity to high-mannose-rich glycoproteins such as HIV gp120 (M.W.D., K.L. Mayer, N.V. Garcia, H. Guo, H. Kajiura, K. Fujiyama, N.M., unpublished data). This implies that a threshold level of high-mannose glycans exists that must be present in proximity in order for AvFc to bind with any appreciable affinity, and non-cancer cells simply may not reach this threshold. Although such a threshold level is unclear at the present time and requires further investigation, the data herein support the notion that AvFc is superior to conventional mannose-specific lectins with respect to selectivity to tumor-associated high-mannose glycans.

Given that changes in *N*-glycosylation modification would globally give rise to any glycoproteins in cancer cells, it is not surprising that the proteomics analysis revealed a large number of proteins recognized by AvFc in A549 and H460 cells (Table 1). Of interest is that EGFR and IGF1R were among the common cell surface glycoproteins targeted by AvFc in these NSCLC cells (Figure 2). The result indicates that these receptors, which are often overexpressed and strongly associated with cancer progression in NSCLC,[23–25] display dense high-mannose glycans on the cancer cells. In fact, they are both highly glycosylated, containing as many as 13 and 16 *N*-glycosylation sites (UniProtKB: P00533 and P08069), respectively. Also, as the ectodomains of EGFR in its activated form and IGF1R exist as dimer,[38–40] it is plausible that AvFc exhibits high affinity for these receptors. In Figure S2, we found that AvFc has higher affinity to EGFR dimer than to EGFR monomer, which suggests that high expression and activation of EGFR on some cancer cell surfaces may increase local high-mannose glycan concentrations and facilitate binding and antitumor activity of AvFc. One of the consequences of AvFc binding to EGFR and IGF1R was the blockade of their activation and subsequent downstream signaling, as demonstrated by the data showing that AvFc inhibited the phosphorylation of both receptors as well as AKT and MAPK1 upon stimulation with their respective ligands in A549 cells (Figures 3A–3G).

The ability of AvFc to inhibit both EGFR and IGF1R has important therapeutic implications, as currently there is no FDA-approved anticancer drug that can simultaneously block these receptors. CTX, an FDA-approved anti-EGFR antibody therapeutic used in the present study as a reference, was only able to block EGFR, but not IGF1R, in A549 (Figures 3 and 4) and, in stark contrast to AvFc, could not exhibit any antitumor effect against the H460 cell line (Figures 4, 5, and 6), which is known to be CTX resistant.[41] The remarkable *in vivo* antitumor efficacy observed with AvFc is most likely due to its effective binding to high-mannose glycans that are broadly and highly accumulated on the surface of cancer cells; in our ongoing study, AvFc showed a similar antitumor effect protecting against B16F10 melanoma lung metastasis, while the non-sugar-binding mutant AvFc^{lec-} failed to show any effect (unpublished data). Despite the fact that colorectal cancer patients show significant improvements in response rates, overall survival, and progression-free survival after CTX treatment, CTX responses in NSCLC patients have not been convincing in clinical trials.[42–44] IGF1R may be involved in the resistance mechanism of CTX and other EGFR-targeted drugs,[45–48] as these two receptors share similar downstream signaling pathways (phosphatidylinositol 3-kinase [PI3K]/AKT/MAPK/nuclear factor κB [NF-κB]); IGF1R can bypass EGFR inhibition, while their cooperation may promote tumor growth and progression.[47–49] One study revealed that overexpression of both EGFR and IGF1R was observed in 24.8% of 125 surgical NSCLC patients, and high co-expression of EGFR and IGF1R was a significant prognostic factor of worse disease-free survival.[49]

To further elucidate the potential antitumor mechanism of action of AvFc, we measured ADCC activities in both reporter-cell-based assays and human-PBMC-based assays (Figures 5A and 5B). In both assay

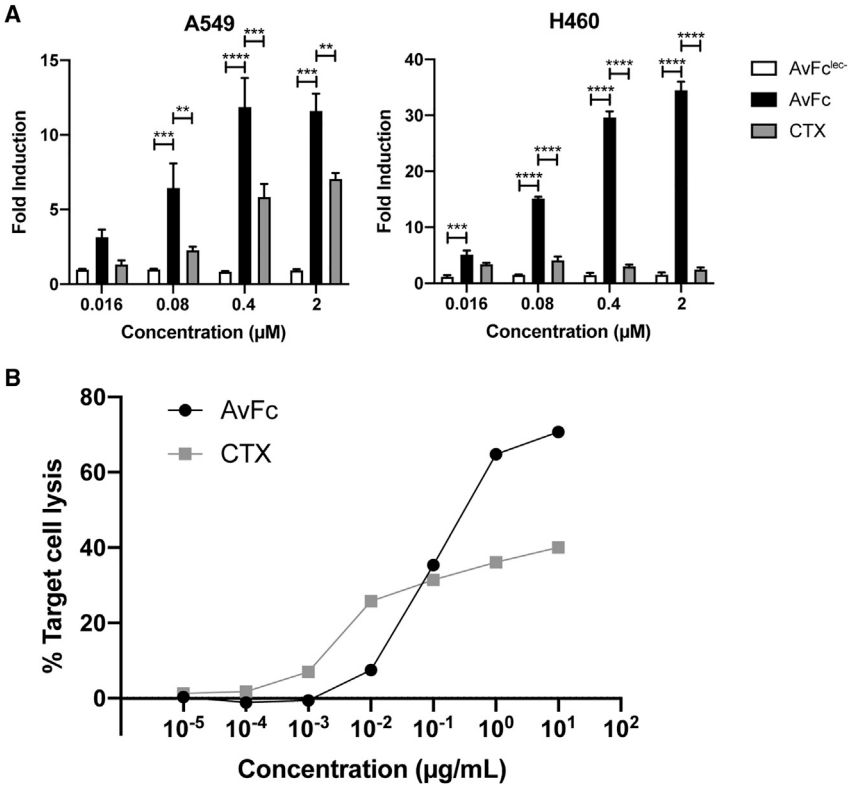

Figure 5. *In vitro* Fc-mediated anticancer activity of AvFc

(A) FcγRIIIa activation by AvFc, AvFc^{lec-} and CTX against A549 or H460 cells in a reporter-cell-based assay. Representative data from at least two independent experiments are shown. Columns and bars represent mean ± SEM (n = 3). Groups were compared with two-way ANOVA followed by Tukey multiple comparison test (**p < 0.01, ***p < 0.001, ****p < 0.0001). (B) Human PBMC-based ADCC assay using A549 lung cancer cells. Cells were pre-incubated with serial dilutions of AvFc or CTX for 30 min in a 37°C/5% CO_2 incubator. PBMCs were added to initiate the ADCC effects at an optimized effector/target ratio (50:1 for AvFc, 25:1 for CTX). After incubation in a 37°C/5% CO_2 incubator for 6 h, cell supernatants were collected for measuring released lactose dehydrogenase to calculate % target cell lysis. The experiment was done in triplicates, with mean ± SEM shown for each data point.

formats, AvFc elicited a strong ADCC response by effectively activating FcγRIIIa on the surface of engineered Jurkat cells (which express luciferase in response to activation) and PBMCs. Conversely, CTX had no activity against H460 cells and only moderate activity against A549 in both the reporter cell assay and PBMC-based assay, underperforming AvFc. This was consistent with the antitumor effects of AvFc seen in Prkdc^{scid}/SzJ (SCID) mice challenged with A549 and H460 xenografts (Figures 6A–6C), wherein AvFc treatment slowed the growth of both xenografts, while CTX was efficacious only against A549. Taken together, these results suggest that binding and inhibition of multiple cell-surface receptors in addition to more potent ADCC activity resulted in superior anticancer activity of AvFc in these models.

The selectivity of AvFc was evaluated in 10 pairs of tumor and adjacent lung tissues from NSCLC patients (Figures 7A–7D). Overall, AvFc interacted preferentially with tumor tissue and was capable of distinguishing the tumor and adjacent tissues, despite the low level of background AvFc staining in the latter. In this initial study, we did not investigate high-mannose expression levels within the tissues, which will likely depend on the developmental stage of the cancer; moreover, we did not evaluate EGFR gene mutations. However, IHC analysis showed that tumors express more EGFR and IGF1R than the adjacent normal tissues (Figure S3), supporting the higher binding of AvFc to tumors. Despite these limitations, the selective interaction of AvFc with primary NSCLC cells in this analysis demonstrates the utility of AvFc beyond animal models and suggests that it may be able to effectively target tumors in NSCLC patients.

While our findings lend support for the notion that high-mannose glycans constitute a cancer glycobiomarker, it remains elusive how or why high-mannose glycans become over-represented on the surface of cancer cells in the first place. A few cellular mechanisms have been identified that allow the accumulation of immature glycans in tumors, including stress-independent activation of X-box binding protein 1 (XBP1), misregulation of N-acetylglucosaminyltransferase, and downregulation of α-mannosidase I and mannosyl(α-1,3-)-glycoprotein β-1,2-N-acetylglucosaminyltransferase (MGAT1).[10,11,50,51] Stress-independent activation of XBP1, for instance, was found to reduce sialylation and bisecting GlcNAc, while increasing the levels of high-mannose glycans in HEK293 and HeLa cells by affecting mannosidase expression.[50] The significant reduction of α-mannosidase I expression found in cholangiocarcinoma cells was correlated to the elevation of high-mannose glycans and a more metastatic phenotype.[11] The use of kifunensine, a small-molecule inhibitor of α-mannosidase I, also increased high-mannose glycan content and produced similar results.[11] Takayama et al. have shown that increased high-mannose glycan expression, detected in surgical specimens of hepatocellular carcinoma, was associated with decreased expression of MGAT1, a key glycosyltransferase that converts high-mannose glycans to complex- or hybrid-type N-glycans.[10] Meanwhile, high-mannose glycans at the helical domain of transferrin receptor protein 1 appear to trigger structural changes that improve noncovalent interaction energies, resulting in cell migration enhancement in metastatic cholangiocarcinoma.[11] A recent publication assessing the impact of high-mannose glycans on bone-marrow-derived mesenchymal stromal cells has provided evidence that these glycans alter the physical and structural properties of the cells themselves, decreasing their size and increasing motility, which may in part explain the greater metastatic potential seen in other cell lines.[52] Given the

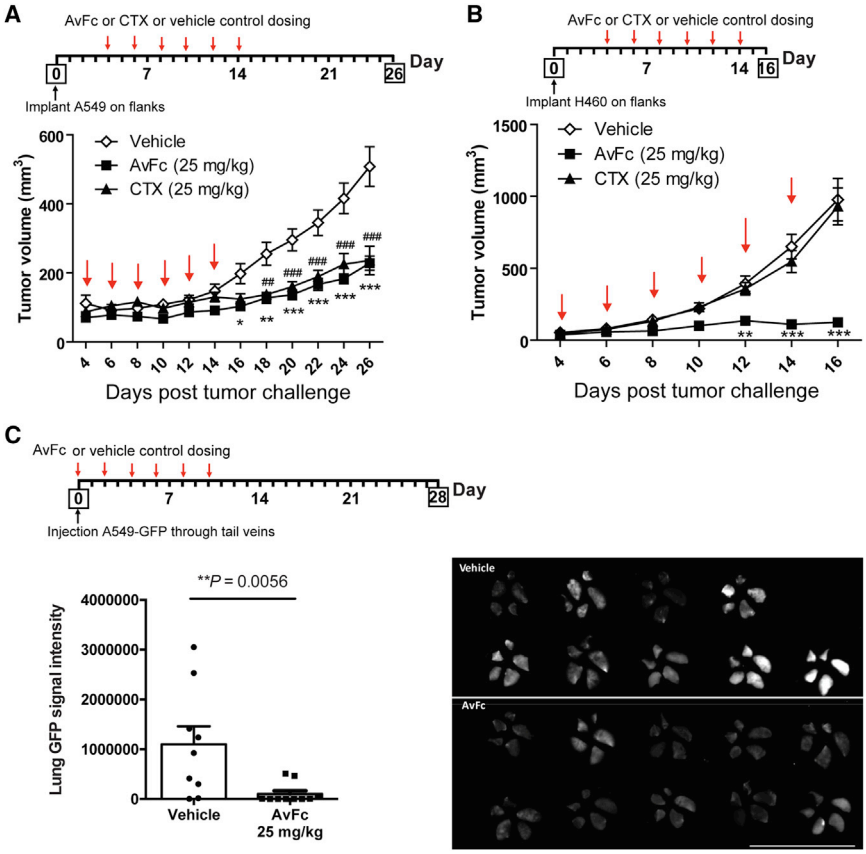

Figure 6. *In vivo* anticancer activity of AvFc

(A and B) The A549 subcutaneous xenograft challenge model (A) and the H460 subcutaneous xenograft challenge model (B) in SCID mice. Four days post challenge, mice were treated i.p. with AvFc or CTX at 25 mg/kg or a vehicle control every other day (Q2D) for a total of 6 doses, as indicated by arrows. Animals were monitored until day 26 for A549 and day 16 for H460 models. Tumor volumes were compared with two-way ANOVA followed by Tukey multiple comparison tests (*p < 0.05, **p < 0.01, ***p < 0.001 between vehicle and AvFc; ##p < 0.01; ###p < 0.001 between vehicle and CTX). (C) The A549-GFP human lung cancer metastasis model in SCID mice. SCID mice were i.v. challenged with A549-GFP cells on day 0, followed by every-other-day dosing with an i.p. injection of AvFc at 25 mg/kg (n = 10) or a vehicle control (n = 9), as indicated in the diagram. On day 35, the lungs were removed, and GFP signal intensity of the lung from each mouse was quantified. Columns and bars represent mean ± SEM, with dots representing individual mice. GFP images of the lungs (4 right and single left lobes) from all animals in vehicle and AvFc groups are shown in the right. Scale bar, 5 cm. Statistical difference between groups was analyzed by the Mann-Whitney test.

growing body of evidence indicating the close association between the abundance of high-mannose glycans on cancer cells and increased cell migration and metastatic potential, it is of high clinical significance to uncover the cause and process leading to high-mannose overexpression in cancer and to scrutinize its functions in tumor microenvironments and metastasis. In this regard, AvFc may provide a valuable tool to probe and monitor high-mannose glycan accumulation on the cell surface, thereby facilitating such investigations.

In summary, the present study demonstrated that AvFc, a lectibody targeting high-mannose glycans, can selectively recognize cancer cells and exert antitumor activity possibly through a combination of growth factor receptor inhibition and immune activation via Fc receptors. Our findings suggest that increased abundance of high-mannose glycans in cancer, such as those expressed on EGFR and IGF1R, can be a druggable target in NSCLC, and AvFc may provide a new tool to probe and target tumor-associated high-mannose glycan biomarker. Further investigation is warranted to confirm the efficacy, safety, and immunogenicity of AvFc for its development as an anticancer agent.

MATERIALS AND METHODS

Human lung tissues

We acquired de-identified postoperative human lung cancer tissues and paired adjacent tissues from University of Louisville Hospital (Louisville, KY). The pathological type of each tumor was determined to be NSCLC. Informed written consent was provided by all participants, and the study protocol was approved by the Human Subjects Protection Program of University of Louisville (Study #18.1240). The distinction between tumor and adjacent tissue was made by the surgeon at the time of tissue removal, and tissues were immediately frozen in liquid nitrogen at surgery and stored at −80°C.

Animal housing and care

Nine-week-old female Prkdc^{scid}/SzJ (SCID) mice (The Jackson Laboratory, Bar Harbor, ME) were housed in a temperature-controlled environment, with an alternating light/dark cycle of 12 h and free access to standard diet and water. The investigators were not blinded for sample administration. All experimental procedures were approved by the University of Louisville Institutional Animal Care and Use Committee.

Reagents

Antibodies specific to EGFR (D38B1), phospho-EGFR (Y1068), IGF1R (D23H3), phospho-IGF1R (Y1131), AKT, phospho-AKT (S473), MAPK1, and phospho-MAPK1 (ERK1/2) were purchased from Cell Signaling Technology (Danvers, MA). EGF and IGF1 were purchased from Thermo Fisher Scientific (Waltham, MA). CTX was obtained from the University of Louisville Hospital pharmacy.

Cell culture

All cell lines were obtained from American Type Culture Collection (ATCC, Manassas, VA) and authenticated by the supplier. Cells

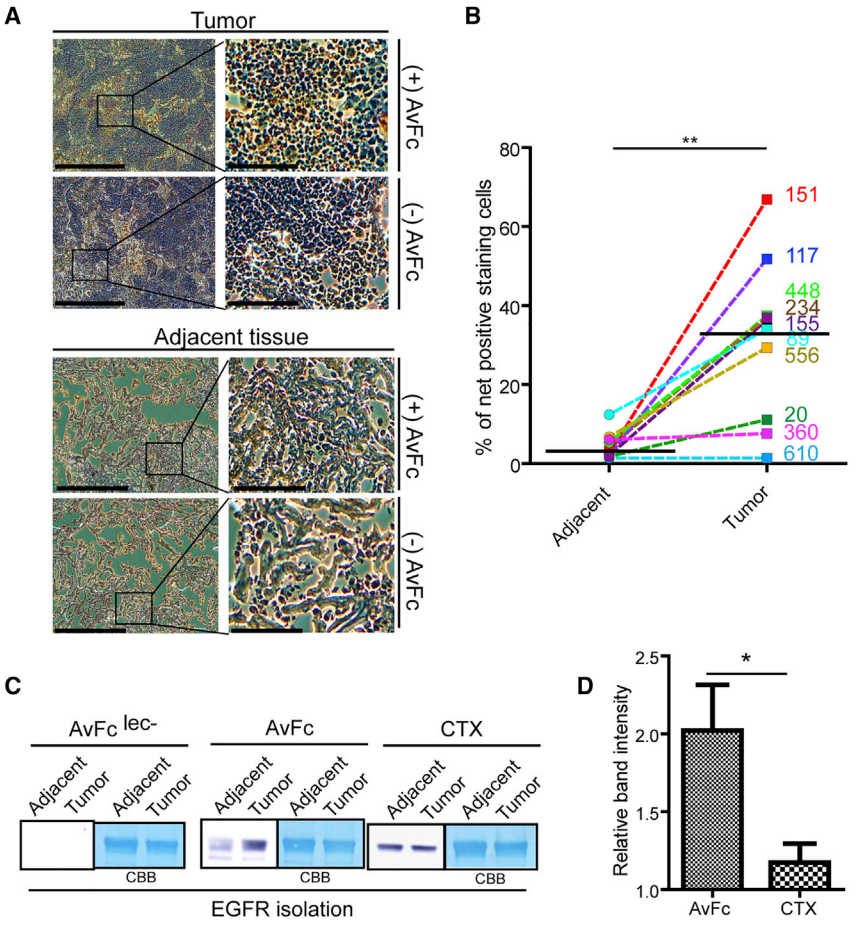

Figure 7. Analysis of AvFc binding to primary human lung tissue and EGFR

Binding to human NSCLC tissue was evaluated using IHC. (A) IHC staining with AvFc or a biotinylated anti-human IgG secondary antibody only. Representative stains from patient 117 lung tissues are shown, with hematoxylin as a counterstain. Scale bar, 200 μm (left image) or 100 μm (right image). (B) Quantification of AvFc staining for lung tissues from all 10 patients tested using ImageJ. The number of positively stained cells between tumor and matched adjacent tissue was compared using the non-parametric Wilcoxon matched-pairs signed rank test (**$p < 0.01$). (C) Representative immunoblot analysis of EGFR isolated from NSCLC tumor or matched adjacent tissue samples from 5 patients. EGFR was isolated by anti-EGFR IgG1 with protein A bead precipitation and detected with AvFc^{lec-}, AvFc, or CTX. CBB, Coomassie Brilliant Blue staining. (D) Quantification of EGFR immunoblot using a densitometry analysis. Relative binding intensities (tumor:adjacent) are shown for AvFc and CTX. Columns and bars represent mean ± SEM (n = 5), and data were compared using an unpaired t test (*$p < 0.05$).

were grown according to ATCC's recommendations, regularly screened for mycoplasma using a commercial PCR-based kit (ATCC) and tested at low passage numbers, with quality ensured based on viability and morphologic inspection. In particular, A549 cells were grown in DMEM supplemented with 10% FBS and 1% penicillin/streptomycin, and H460 cells were grown in RPMI 1640 supplemented with 10% FBS and 1% penicillin/streptomycin unless otherwise stated.

Production of AvFc

AvFc and AvFc^{lec-} were produced using a transient plant expression vector in *Nicotiana benthamiana* as described previously.[18] Briefly, 4-week-old plants were transformed with a magnICON vector containing the gene for AvFc by agroinfiltration and incubated for 1 week. At that time, leaf tissue was homogenized in a NaPi buffer at a pH of 7.4 and clarified by centrifugation, followed by fast protein liquid chromatography on the ÄKTA pure system (GE Healthcare Life Sciences, Chicago, IL) using protein A as the first chromatography step and ceramic hydroxyapatite (CHT) as a cleanup step. Endotoxin was removed from the purified protein using the Triton X-114 phase separation method, followed by concentration of the protein using a 10 kDa MWCO centrifugal filter and sterilization with a 0.2 μm filter. Purity was assessed with SDS-PAGE, with AvFc appearing as a band at approximately 77 kDa under non-reducing conditions.

Flow cytometry analysis of AvFc binding to human cells

Cancer cell lines were harvested and incubated with various concentrations of AvFc (0.1 μg/mL, 1 μg/mL, and 10 μg/mL) in culture medium for 30 min on ice and washed 3 times with DPBS. Cells were then incubated with goat F(ab′)2 anti-Human IgG Fc-FITC antibody (Abcam, Cambridge, MA) for 30 min in the dark on ice. After washing 3 additional times with Dulbecco's phosphate-buffered saline (DPBS), the cells were fixed with 1% formalin for 15 min on ice. Data were acquired on a FACSCalibur flow cytometer (BD BioSciences, San Jose, CA) by counting 10,000 events per sample and determining the percentage of FITC$^+$ cells with FlowJo. The non-sugar-binding mutant AvFc^{lec-} was used as a negative control. The analyses were performed in triplicate.

Immunofluorescence

For immunofluorescence, 1,000 A549 cells or 10,000 BEAS-2B cells were seeded per chamber in Lab-Tek II chamber slides (Thermo Fisher Scientific, Waltham, MA) and incubated for 24 h. After washing with PBS, cells were fixed in 4% formalin in PBS for 20 min at room temperature. After incubation with 0.2% Triton X-100 in PBS for 15 min at room temperature, Human Fc Block (BD, San Jose, CA) was added to cells and incubated for an additional 10 min. Cells were then blocked with 3% BSA-PBS for 30 min at room temperature and then incubated with 250 units of endoglycosidase H

at 37°C for 1 h, according to the manufacturer's protocol (New England Biolabs, Ipswich, MA). Cells were then stained with 10 μg/mL of AvFc for 3 h at room temperature and, after washing with PBS, stained with a 1:40 dilution of anti-human IgG-FITC (Sigma, Mendota Heights, MN) for 1 h at room temperature. Cells were then mounted with coverslips using mounting medium for fluorescence with DAPI (VECTASHIELD®, Burlingame, CA). Slides were analyzed by fluorescent confocal microscopy (ZEISS LSM 880).

Co-immunoprecipitation

For co-immunoprecipitation, 1×10^6 A549 or H460 cells were seeded in a 10 cm^2 plate (Corning, Tewksbury, MA) and incubated in growth medium for 24 h. Cells were washed with PBS, and cell lysates were prepared in T-PER buffer (Thermo Fisher Scientific, Waltham, MA) supplemented with a protease/phosphatase inhibitor (Thermo Fisher Scientific, Waltham, MA). After centrifugation at 13,000 × *g* for 10 min at 4°C, supernatants were mixed with 4 μg of AvFc or $AvFc^{-lec}$. After incubation for 24 h at 4°C, 10 μL of protein A beads (Santa Cruz, Dallas, TX) was added. After an additional incubation for 2 h at 4°C, the mixture was washed with T-PER buffer and immunoblot analysis was performed.

EGFR isolation

Tissue homogenates were prepared by silicon beads and Precellys 24 homogenizer (Bertin, Rockville, MA) in T-PER buffer (Thermo Fisher Scientific, Waltham, MA) with protease inhibitor cocktail (Sigma, Mendota Heights, MN). Debris were removed by centrifugation at 13,000 × *g* for 10 min at 4°C. Supernatants were incubated with 4 μg of Anti-EGFR IgG1 (D38B1) (Cell Signaling Technology, Danver, MA) and 20 μg of protein A beads (Santa Cruz, Dallas, TX) for 4 h at 4°C. The mixture was washed with T-PER buffer.

Immunoblot analysis

SDS-PAGE and membrane transfer cassettes were purchased from Thermo Fisher Scientific (Waltham, MA). Protein samples were run on 10% Bolt Bis-Tris Plus gels with NuPAGE MES SDS running buffer (Thermo Fisher Scientific, Waltham, MA). Transfer to polyvinylidene fluoride (PVDF) membranes in NuPAGE transfer buffer was carried out at 10 V overnight at 4°C. Membranes were then incubated in 3% BSA in Tris-buffered saline supplemented with 0.01% Triton X-100 (TBST) for 2 h, and anti-EGFR, anti-IGF1R, anti-human Fc, or AvFc in TBST supplemented with 1% BSA was incubated overnight at 4°C. Horseradish-peroxidase-tagged secondary antibodies (Anti-rabbit IgG, Santa Cruz, Dallas, TX; Anti-human IgG, SouthernBiotech, Birmingham, AL) were used for protein detection, and membrane images were taken using Amersham Imager 600 (GE Healthcare Life Sciences, Chicago, IL).

Proteomics analysis

Potential cell-surface binding partners of AvFc were identified using co-immunoprecipitation followed by mass spectrometry. Co-immunoprecipitation in this instance was performed using the Pierce Co-immunoprecipitation Kit (Thermo Fisher Scientific, Waltham, MA) according to the manufacturer's instructions. Briefly, whole-cell lysates of A549 and H460 cells were pre-cleared with a control agarose resin to reduce non-specific interactions, then co-incubated with 100 μg of AvFc or $AvFc^{lec-}$, which were covalently attached to an agarose resin for 2 h at 4°C. Bound proteins were then eluted using a low pH buffer and neutralized with 1 M tris base for mass spectrometry analysis.

Protein samples were digested with trypsin (1:50 ratio) in a filter-aided sample preparation approach following reduction and alkylation with 100 mM dithiothreitol and 50 mM iodoacetamide. The tryptic digests (0.5 μg) were separated using a Proxeon EASY n-LC (Thermo Fisher Scientific, Waltham, MA) UHPLC system and Dionex (Sunnyvale, CA) 2 cm Acclaim PepMap 100 trap and a 15 cm Dionex Acclaim PepMap RSLC (C18, 2 μm, 100 Å) separating column. The eluate was introduced into an LTQ-Orbitrap ELITE (Thermo Fisher Scientific, Waltham, MA) using a Nanospray Flex source and MS2 data collected in a data-dependent fashion in a top-20 rapid CID method. All MS1 data were acquired using Fourier transform ion cyclotron resonance mass spectrometry at 240,000 resolution and MS2 data using the linear ion trap. MSn data were searched using Proteome Discoverer 1.4 (Thermo Fisher Scientific, Waltham, MA) with Sequest HT (SageN) and Mascot, version 4.0 (Matrix Science) in a decoy database search strategy against UniProt Knowledgebase, *Homo sapiens* reference proteome. The searches were performed with a fragment ion mass tolerance of 1.0 Da and a parent ion tolerance of 50 ppm. The search data results file was imported into Scaffold, v.4.3.4 (Proteome Software Inc.) and filtered using a 2 ppm mass error filter, removal of decoy hits, to control for <1.0% false discovery rates with PeptideProphet and ProteinProphet (Institute for Systems Biology). Peptide and protein identifications were accepted at >95.0% probability by the PeptideProphet or ProteinProphet algorithm. A comparison of protein abundance among the sample sets was conducted in Scaffold using the intensity-based absolute quantification (iBAQ) method. Results were further refined using Gene Ontology (GO) terms to extract the most abundant membrane receptors, transporters, and adhesion molecules bound by AvFc and not $AvFc^{lec-}$.

Transwell migration assay

For transwell migration assay, 1×10^5 A549 or H460 cells in 200 μL of serum-free growth medium were seeded in the insert of a transwell plate with 8 μm pores (VWR International, Radnor, PA). These cells were co-incubated with AvFc or CTX at 30 nM for 2 h at 37°C. Afterward, growth medium supplemented with 20% FBS was added to the outside well, and EGF or IGF-1 was added to a final concentration of 2 ng/mL in the transwell insert. After 6 h, migrated cell counts were determined by trypsinization and trypan blue staining (Thermo Fisher Scientific, Waltham, MA).

ADCC reporter assay

ADCC was assessed by an ADCC Reporter Bioassay (Promega, Madison, WI) following the manufacturer's protocol. Each sample was tested in triplicate. Briefly, 3 NSCLC cell lines used as target cells

were seeded in an opaque white 96-well flat-bottom culture plate (Corning, Tewksbury, MA) at 10,000[4] cells/well and incubated at 37°C with 5% CO_2. At 24 h later, various concentrations of AvFc, AvFc^{lec-}, or CTX were added to target cells along with the Jurkat NFAT-luc FcγRIIIa-expressing cell line (Jur-FcγRIIIa; Promega, Madison, WI) at a ratio of 15:1. FcγRIIIa signaling activates the NFAT transcription factor, inducing the expression of firefly luciferase through an NFAT responsive promoter. After co-culture for 24 h, firefly luciferase activity was measured using the Britelite Plus Reporter Gene Assay System (PerkinElmer, Waltham, MA) on a Synergy HT luminometer (BioTeck, Winooski, VT). Jur-FcγRIIIa cells co-cultured with the target cells in the absence of antibody provided no antibody control luciferase production levels, which were subtracted from the actual signals to yield antibody-specific activation, in relative light units (RLUs). Background was determined by taking the mean of the target-cell-only wells. Fold induction was calculated using the following equation: Fold induction = $(RLU_{induced} - RLU_{background})/(RLU_{noAbcontrol} - RLU_{background})$.

ADCC assay with primary human PBMC effector cells

Similar to the reporter assay, plated A549 target cells were pre-incubated with serial dilutions of AvFc or CTX for 30 min at 37°C. PBMCs were added to initiate the ADCC at ratio of 50:1 for AvFc and 25:1 for CTX. After incubation at 37°C incubator for 6 h, cell supernatants were collected, and released lactose dehydrogenase was measured and compared to a no-drug control to calculate percent target cell lysis. Each sample was tested in triplicate.

Subcutaneous lung cancer xenograft challenge model

Using 8-week-old female SCID mice, 1×10^7 A549 cells or 5×10^5 H460 were implanted into the hind left flanks. The mice were then randomly organized into 3 groups and treated with the vehicle (n = 10), 25 mg/kg AvFc (n = 10), and 25 mg/kg CTX (n = 10). Vehicle treatment consisted of the AvFc formulation buffer (30 mM histidine pH 7.4, 100 mM sucrose, 100 mM NaCl). Treatments were administered intraperitoneally (i.p.) on days 4, 6, 8, 10, 12, and 14 following the formation of palpable lesions. Body weights and tumor volumes were measured every other day after treatment. Animals were euthanized 26 days after A549 challenge and 16 days after H460 challenge.

A549 lung metastasis model

A549 cells expressing GFP were grown to confluency in growth medium. After harvest, 2×10^6 cells were injected intravenously (i.v.) into 9-week-old female SCID mice. The mice were then randomly organized into 2 groups and treated with the vehicle (n = 10) and 25 mg/kg AvFc (n = 10). Treatments were administered i.p. on days 0, 2, 4, 6, 8, and 10. Following treatment, mice were weighed every other day. Finally, the animals were euthanized on day 28, with the lungs surgically removed and fixed in 10% formalin. To detect GFP signals, each lobe of lungs was separated, and GFP signals were detected by Amersham Imager 600 (GE Healthcare Life Sciences, Chicago, IL).

Immunohistochemistry

Immunohistochemical staining was performed on the cryosections of frozen tissues from lung cancer patients undergoing surgery. Staining was performed with the VECTASTAIN Elite ABC HRP Kit (Peroxidase, Standard) (Vector Labs, Burlingame, CA). Then, 8 μm tissue sections were placed on positively charged slides (VWR International, Radnor, PA) and air dried. The sections were incubated for 10 min at room temperature in 3% H_2O_2 diluted in methanol and washed with TBST. Avidin/biotin blockade was performed using a blocking kit for 15 min at room temperature (Abcam, Cambridge, MA), then Fc receptors were blocked in Fc-blocking solution for 10 min at room temperature (BD, San Jose, CA). Sections were further blocked with 3% goat serum in TBST for 30 min at room temperature. To stain the tissue, 0.5 μg/mL of AvFc in TBST supplemented with 1% goat serum was added for 30 min at room temperature, followed by a biotinylated anti-human IgG in TBST with 1% goat serum also incubated for 30 min at room temperature (Vector Labs, Burlingame, CA). Then, ABC solution was added for 30 min at room temperature (Vector Labs, Burlingame, CA) followed by the DAB stain, which was applied following the manufacturer's protocol (Vector Labs, Burlingame, CA). Sections were washed between each step 3 times with TBST. Counterstaining was performed with hematoxylin. Sections were serially dehydrated with 95% ethanol, 100% ethanol, and CitriSolv (Decon Laboratories, King of Prussia, PA). Images were taken using an OLYMPUS CKX41 microscope with UPlanFL 10×/0.30 lens (Olympus, Tokyo, Japan).

Statistical analyses

Group means and standard errors were derived from the values obtained in 3 individual replicates, and assays were performed at least twice independently unless otherwise noted. For all data, outliers were determined by statistical analysis using the Grubb test ($p < 0.05$) and excluded from further analysis. Statistical significance was analyzed by one-way or two-way analysis of variance (ANOVA) with Bonferroni post hoc test or Wilcoxon matched-pairs signed rank test as indicated in figure legends, using GraphPad Prism 5 (San Diego, CA). Differences were considered statistically significant if $p < 0.05$.

Data availability

All data generated during or analyzed during the current study are available from the corresponding author on reasonable request.

SUPPLEMENTAL INFORMATION

Supplemental information can be found online at https://doi.org/10.1016/j.ymthe.2022.01.030.

ACKNOWLEDGMENTS

We thank J. Calvin Kouokam, Rachel Carry, and Sucheta Telang for useful discussion and technical assistance and Victor Van Berkel for his support in acquisition of human lung cancer tissues. This work was supported by an NIH grant (R21-CA216447), a U.S. Department of Defense grant (W81XWH-10-2-0082-CLIN2), and a University of Louisville Brown Cancer Center Molecular Target CoBRE grant (as a

subproject of NIH NIGMS/P30-GM106396). M.W.D. was supported by a T32 Environmental Health Sciences Grant (T32-ES011564).

AUTHOR CONTRIBUTIONS

Y.J.O., M.W.D., and N.M. wrote the manuscript. Y.J.O. performed experiments. M.W.D. and A.R.F. assisted to perform parts of experiments. M.L.M. performed proteomics analysis. Y.J.O., M.W.D., Q.Z., M.L.M, C.B.L., and N.M. analyzed data. N.M. conceived and designed experiments, secured funding, and supervised the study.

DECLARATION OF INTEREST

N.M. filed a patent application related to this work (PCT/US2018/017617).

REFERENCES

1. Loke, I., Kolarich, D., Packer, N.H., and Thaysen-Andersen, M. (2016). Emerging roles of protein mannosylation in inflammation and infection. Mol. Aspects Med. *51*, 31–55.
2. Oliveira-Ferrer, L., Legler, K., and Milde-Langosch, K. (2017). Role of protein glycosylation in cancer metastasis. Semin. Cancer Biol. *44*, 141–152.
3. Pearce, O.M.T. (2018). Cancer glycan epitopes: biosynthesis, structure and function. Glycobiology *28*, 670–696.
4. de Leoz, M.L., Young, L.J., An, H.J., Kronewitter, S.R., Kim, J., Miyamoto, S., Borowsky, A.D., Chew, H.K., and Lebrilla, C.B. (2010). High-mannose glycans are elevated during breast cancer progression. Mol. Cell. Proteomics *10*, M110.002717.
5. Liu, X., Nie, H., Zhang, Y., Yao, Y., Maitikabili, A., Qu, Y., Shi, S., Chen, C., and Li, Y. (2013). Cell surface-specific N-glycan profiling in breast cancer. PLoS One *8*, e72704.
6. Sethi, M.K., Hancock, W.S., and Fanayan, S. (2016). Identifying N-glycan biomarkers in colorectal cancer by mass spectrometry. Acc. Chem. Res. *49*, 2099–2106.
7. Chik, J.H., Zhou, J., Moh, E.S., Christopherson, R., Clarke, S.J., Molloy, M.P., and Packer, N.H. (2014). Comprehensive glycomics comparison between colon cancer cell cultures and tumours: implications for biomarker studies. J. Proteomics *108*, 146–162.
8. Boyaval, F., Van Zeijl, R., Dalebout, H., Holst, S., van Pelt, G., Farina-Sarasqueta, A., et al. (2021). N-glycomic signature of stage II colorectal cancer and its association with the tumor microenvironment. Mol. Cell. Proteomics *20*, 100057.
9. Powers, T.W., Holst, S., Wuhrer, M., Mehta, A.S., and Drake, R.R. (2015). Two-Dimensional N-glycan distribution mapping of hepatocellular carcinoma tissues by MALDI-imaging mass spectrometry. Biomolecules *5*, 2554–2572.
10. Takayama, H., Ohta, M., Iwashita, Y., Uchida, H., Shitomi, Y., Yada, K., and Inomata, M. (2020). Altered glycosylation associated with dedifferentiation of hepatocellular carcinoma: a lectin microarray-based study. BMC Cancer *20*, 192.
11. Park, D.D., Phoomak, C., Xu, G., Olney, L.P., Tran, K.A., Park, S.S., Haigh, N.E., Luxardi, G., Lert-Itthiporn, W., Shimoda, M., et al. (2020). Metastasis of cholangiocarcinoma is promoted by extended high-mannose glycans. Proc. Natl. Acad. Sci. U S A *117*, 7633–7644.
12. Ruhaak, L.R., Taylor, S.L., Stroble, C., Nguyen, U.T., Parker, E.A., Song, T., Lebrilla, C.B., Rom, W.N., Pass, H., Kim, K., et al. (2015). Differential N-glycosylation patterns in lung adenocarcinoma tissue. J. Proteome Res. *14*, 4538–4549.
13. Park, H.M., Hwang, M.P., Kim, Y.W., Kim, K.J., Jin, J.M., Kim, Y.H., Yang, Y.-H., Lee, K.H., and Kim, Y.-G. (2015). Mass spectrometry-based N-linked glycomic profiling as a means for tracking pancreatic cancer metastasis. Carbohydr. Res. *413*, 5–11.
14. Everest-Dass, A.V., Briggs, M.T., Kaur, G., Oehler, M.K., Hoffmann, P., and Packer, N.H. (2016). N-glycan MALDI imaging mass spectrometry on formalin-fixed paraffin-embedded tissue enables the delineation of ovarian cancer tissues. Mol. Cell. Proteomics *15*, 3003–3016.
15. Chen, H., Deng, Z., Huang, C., Wu, H., Zhao, X., and Li, Y. (2017). Mass spectrometric profiling reveals association of N-glycan patterns with epithelial ovarian cancer progression. Tumour Biol. *39*, 1010428317716249.
16. Munkley, J., Mills, I.G., and Elliott, D.J. (2016). The role of glycans in the development and progression of prostate cancer. Nat. Rev. Urol. *13*, 324–333.
17. Moginger, U., Grunewald, S., Hennig, R., Kuo, C.W., Schirmeister, F., Voth, H., Rapp, E., Khoo, K.-H., Seeberger, P.H., Simon, J.C., and Kolarich, D. (2018). Alterations of the human skin N- and O-glycome in basal cell carcinoma and squamous cell carcinoma. Front. Oncol. *8*, 70.
18. Hamorsky, K.T., Kouokam, J.C., Dent, M.W., Grooms, T.N., Husk, A.S., Hume, S.D., Rogers, K.A., Villinger, F., Morris, M.K., Hanson, C.V., and Matoba, N. (2019). Engineering of a lectibody targeting high-mannose-type glycans of the HIV envelope. Mol. Ther. *27*, 2038–2052.
19. Matoba, N., Husk, A.S., Barnett, B.W., Pickel, M.M., Arntzen, C.J., Montefiori, D.C., Takahashi, A., Tanno, K., Omura, S., Cao, H., et al. (2010). HIV-1 neutralization profile and plant-based recombinant expression of actinohivin, an Env glycan-specific lectin devoid of T-cell mitogenic activity. PLoS One *5*, e11143.
20. Seber Kasinger, L.E., Dent, M.W., Mahajan, G., Hamorsky, K.T., and Matoba, N. (2019). A novel anti-HIV-1 bispecific bNAb-lectin fusion protein engineered in a plant-based transient expression system. Plant Biotechnol. J. *17*, 1646–1656.
21. Dent, M., Hamorsky, K., Vausselin, T., Dubuisson, J., Miyata, Y., Morikawa, Y., and Matoba, N. (2020). Safety and efficacy of Avaren-Fc lectibody targeting HCV high-mannose glycans in a human liver chimeric mouse model. Cell. Mol. Gastroenterol. Hepatol. *11*, 185.
22. Maley, F., Trimble, R.B., Tarentino, A.L., and Plummer, T.H., Jr. (1989). Characterization of glycoproteins and their associated oligosaccharides through the use of endoglycosidases. Anal. Biochem. *180*, 195–204.
23. Ludovini, V., Bellezza, G., Pistola, L., Bianconi, F., Di Carlo, L., Sidoni, A., Semeraro, A., Sordo, R.D., Tofanetti, F.R., Mameli, M.G., et al. (2009). High coexpression of both insulin-like growth factor receptor-1 (IGFR-1) and epidermal growth factor receptor (EGFR) is associated with shorter disease-free survival in resected non-small-cell lung cancer patients. Ann. Oncol. *20*, 842–849.
24. Janku, F., Garrido-Laguna, I., Petruzelka, L.B., Stewart, D.J., and Kurzrock, R. (2011). Novel therapeutic targets in non-small cell lung cancer. J. Thorac. Oncol. *6*, 1601–1612.
25. Yeo, C.D., Park, K.H., Park, C.K., Lee, S.H., Kim, S.J., Yoon, H.K., Lee, Y.S., Lee, E.J., Lee, K.Y., and Kim, T.-J. (2015). Expression of insulin-like growth factor 1 receptor (IGF-1R) predicts poor responses to epidermal growth factor receptor (EGFR) tyrosine kinase inhibitors in non-small cell lung cancer patients harboring activating EGFR mutations. Lung Cancer *87*, 311–317.
26. Downward, J., Parker, P., and Waterfield, M.D. (1984). Autophosphorylation sites on the epidermal growth factor receptor. Nature *311*, 483–485.
27. Gates, R.E., and King, L.E., Jr. (1985). Different forms of the epidermal growth factor receptor kinase have different autophosphorylation sites. Biochemistry *24*, 5209–5215.
28. Xu, Q., Malecka, K.L., Fink, L., Jordan, E.J., Duffy, E., Kolander, S., Peterson, J.R., and Dunbrack, R.L., Jr. (2015). Identifying three-dimensional structures of autophosphorylation complexes in crystals of protein kinases. Sci. Signal. *8*, rs13.
29. Laron, Z. (2001). Insulin-like growth factor 1 (IGF-1): a growth hormone. Mol. Pathol. *54*, 311–316.
30. Liu, Q., Guan, J.Z., Sun, Y., Le, Z., Zhang, P., Yu, D., and Liu, Y. (2017). Insulin-like growth factor 1 receptor-mediated cell survival in hypoxia depends on the promotion of autophagy via suppression of the PI3K/Akt/mTOR signaling pathway. Mol. Med. Rep. *15*, 2136–2142.
31. Zheng, W.H., and Quirion, R. (2006). Insulin-like growth factor-1 (IGF-1) induces the activation/phosphorylation of Akt kinase and cAMP response element-binding protein (CREB) by activating different signaling pathways in PC12 cells. BMC Neurosci. *7*, 51.
32. Yarden, Y. (2001). The EGFR family and its ligands in human cancer. signalling mechanisms and therapeutic opportunities. Eur. J. Cancer *37*, S3–S8.
33. Engelman, J.A., and Cantley, L.C. (2006). The role of the ErbB family members in non-small cell lung cancers sensitive to epidermal growth factor receptor kinase inhibitors. Clin. Cancer Res. *12*, 4372s–4376s.
34. Friedl, P., and Wolf, K. (2003). Tumour-cell invasion and migration: diversity and escape mechanisms. Nat. Rev. Cancer *3*, 362–374.

35. Gentilini, D., Busacca, M., Di Francesco, S., Vignali, M., Vigano, P., and Di Blasio, A.M. (2007). PI3K/Akt and ERK1/2 signalling pathways are involved in endometrial cell migration induced by 17beta-estradiol and growth factors. Mol. Hum. Reprod. *13*, 317–322.

36. Newsom-Davis, T.E., Wang, D., Steinman, L., Chen, P.F., Wang, L.X., Simon, A.K., and Screaton, G.R. (2009). Enhanced immune recognition of cryptic glycan markers in human tumors. Cancer Res. *69*, 2018–2025.

37. Kiernan, J.A. (1975). Localization of alpha-D-glucosyl and alpha-D-mannosyl groups of mucosubstances with concanavalin A and horseradish peroxidase. Histochemistry *44*, 39–45.

38. Li, J., Choi, E., Yu, H., and Bai, X.C. (2019). Structural basis of the activation of type 1 insulin-like growth factor receptor. Nat. Commun. *10*, 4567.

39. Kavran, J.M., McCabe, J.M., Byrne, P.O., Connacher, M.K., Wang, Z., Ramek, A., Sarabipour, S., Shan, Y., Shaw, D.E., Hristova, K., et al. (2014). How IGF-1 activates its receptor. Elife *3*, e03772.

40. Liu, P., Cleveland, T.E., 4th, Bouyain, S., Byrne, P.O., Longo, P.A., and Leahy, D.J. (2012). A single ligand is sufficient to activate EGFR dimers. Proc. Natl. Acad. Sci. U S A *109*, 10861–10866.

41. Steiner, P., Joynes, C., Bassi, R., Wang, S., Tonra, J.R., Hadari, Y.R., and Hicklin, D.J. (2007). Tumor growth inhibition with cetuximab and chemotherapy in non-small cell lung cancer xenografts expressing wild-type and mutated epidermal growth factor receptor. Clin. Cancer Res. *13*, 1540–1551.

42. Pujol, J.L., Pirker, R., Lynch, T.J., Butts, C.A., Rosell, R., Shepherd, F.A., Vansteenkiste, J., O'Byrne, K.J., de Blas, B., Heighway, J., et al. (2014). Meta-analysis of individual patient data from randomized trials of chemotherapy plus cetuximab as first-line treatment for advanced non-small cell lung cancer. Lung Cancer *83*, 211–218.

43. Pirker, R., Pereira, J.R., von Pawel, J., Krzakowski, M., Ramlau, R., Park, K., Marinis, F., Eberhardt, W.E.E., Paz-Ares, L., Störkel, S., et al. (2012). EGFR expression as a predictor of survival for first-line chemotherapy plus cetuximab in patients with advanced non-small-cell lung cancer: analysis of data from the phase 3 FLEX study. Lancet Oncol. *13*, 33–42.

44. Pirker, R., Pereira, J.R., Szczesna, A., von Pawel, J., Krzakowski, M., Ramlau, R., Vynnychenko, I., Park, K., Yu, C.-T., Ganul, V., et al. (2009). Cetuximab plus chemotherapy in patients with advanced non-small-cell lung cancer (FLEX): an open-label randomised phase III trial. Lancet *373*, 1525–1531.

45. Morgillo, F., Kim, W.Y., Kim, E.S., Ciardiello, F., Hong, W.K., and Lee, H.Y. (2007). Implication of the insulin-like growth factor-IR pathway in the resistance of non-small cell lung cancer cells to treatment with gefitinib. Clin. Cancer Res. *13*, 2795–2803.

46. Kjaer, I., Lindsted, T., Frohlich, C., Olsen, J.V., Horak, I.D., Kragh, M., and Pedersen, M.W. (2016). Cetuximab resistance in squamous carcinomas of the upper aerodigestive tract is driven by receptor tyrosine kinase plasticity: potential for mAb mixtures. Mol. Cancer Ther. *15*, 1614–1626.

47. Huang, F., Xu, L.A., and Khambata-Ford, S. (2012). Correlation between gene expression of IGF-1R pathway markers and cetuximab benefit in metastatic colorectal cancer. Clin. Cancer Res. *18*, 1156–1166.

48. Guo, X.F., Zhu, X.F., Cao, H.Y., Zhong, G.S., Li, L., Deng, B.G., Chen, P., Wang, P.-Z., Miao, Q.-F., and Zhen, Y.-S. (2017). A bispecific enediyne-energized fusion protein targeting both epidermal growth factor receptor and insulin-like growth factor 1 receptor showing enhanced antitumor efficacy against non-small cell lung cancer. Oncotarget *8*, 27286–27299.

49. Al-Saad, S., Richardsen, E., Kilvaer, T.K., Donnem, T., Andersen, S., Khanehkenari, M., Bremnes, R.M., and Busund, L.-T. (2017). The impact of MET, IGF-1, IGF1R expression and EGFR mutations on survival of patients with non-small-cell lung cancer. PLoS One *12*, e0181527.

50. Wong, M.Y., Chen, K., Antonopoulos, A., Kasper, B.T., Dewal, M.B., Taylor, R.J., Whittaker, C.A., Hein, P.P., Dell, A., Genereux, J.C., et al. (2018). XBP1s activation can globally remodel N-glycan structure distribution patterns. Proc. Natl. Acad. Sci. U S A *115*, E10089–E10098.

51. Zhang, G., Isaji, T., Xu, Z., Lu, X., Fukuda, T., and Gu, J. (2019). N-acetylglucosaminyltransferase-I as a novel regulator of epithelial-mesenchymal transition. FASEB J. *33*, 2823–2835.

52. Alonso-Garcia, V., Chaboya, C., Li, Q., Le, B., Congleton, T.J., Florez, J., Tran, V., Liu, G.-Y., Yao, W., Lebrilla, C.B., and Fierro, F.A. (2020). High mannose N-glycans promote migration of bone-marrow-derived mesenchymal stromal cells. Int. J. Mol. Sci. *21*, 7194.